Destabilization dynamics of clay and acid-free polymers of ferric and magnesium salts in AMD without pH adjustment

I. O. Ntwampe, F. B. Waanders and J. R. Bunt

ABSTRACT

The physicochemical treatment was employed to treat acid mine drainage (AMD) in the removal of turbid materials using clay only (exp A) and a combination of clay, $FeCl_3$ and $Mg(OH)_2$ (exp B) to form a polymer. A 5 g sample of clay (bentonite) was added to 1.2 L of AMD and treated in a jar test at 250 rpm for 2 min and reduced to 100 rpm for 10 min. A 200 mL sub-sample from the 1.2 L mother liquor was poured into five 500 mL glass beakers, and 20 mL dosages of a polymer of 0.1 M Fe^{3+} in ($FeCl_3$) and 0.1 M Mg^{2+} in ($Mg(OH)_2$) was added to the beakers. The samples were allowed to settle for 1 h, after which the supernatant was analyzed for pH, total suspended solids (TSS), dissolved oxygen (DO) and oxidation-reduction potential (ORP) (exp A). A similar set of experiments was conducted where 200 mL of the AMD sample was poured into 500 mL glass beakers and (20–60 mL) dosages of a combination of 5 g clay, 0.1 M Fe^{3+} ($FeCl_3$) and Mg^{2+} ($Mg(OH)_2$) polymer was added and similar mixing, settling time and measurements were conducted (exp B). The polymers used in exp A exhibited TSS removal efficiency (E%) which was slightly lower compared with the polymer used in exp B, above 90%. Clay has a high TSS removal efficiency in the treatment of the AMD, indicating that adsorption was a predominant process in exps A and B. The scanning electron microscope (SEM) micrographs of the AMD sludge of both exps A and B, with a rigid and compacted structure consisting of dense flocs surrounded by the smaller flocs bound together, corroborate the fact that adsorption is a predominant process.

Key words | AMD, clay, coal, DO, dosage, pH, settle, TSS

I. O. Ntwampe (corresponding author)
F. B. Waanders
J. R. Bunt
School of Chemical and Minerals Engineering,
North West University, Faculty of Engineering,
North West Province,
Potchefstroom Campus,
South Africa
E-mail: *ontwampe@gmail.com*

INTRODUCTION

Acid mine drainage (AMD) is characterized by a low pH, high concentrations of sulphates and various heavy metals, making AMD treatment a major concern because of possible deleterious effects of the effluent on the surroundings. The varying mineral content causes the AMD to form a complex solution which requires an intensive treatment approach. The low pH of the AMD contributes to the high solubility of the toxic metals, which then permits their dispersion into the environment (Hallberg 2010). It contains different minerals and also has a high ionic movement, which results in a highly reactive tendency (Skalny *et al.* 2001; Nielsen *et al.* 2005; Edwards & Withers 2007; Firer *et al.* 2008; Nielsen *et al.* 2008a, 2008b; Sinha *et al.* 2013). Its low pH results from the sulphuric acid, which is derived from the oxidation of the iron sulphides (FeS_x), particularly pyrite (FeS_2), by oxygen in an aqueous environment (Gupta 2007; Cravotta 2008; Huang & Finkelman 2008; Hower *et al.* 2008; Silva *et al.* 2009; Gallato *et al.* 2009; Silva *et al.* 2010), as shown by Equation (1).

$$2\,FeS_2 + 7O_2 + 2H_2O \rightarrow 2Fe^{2+} + 4SO_4^{2-} + 4H^+ \quad (1)$$

The iron sulphide is a naturally occurring compound embedded in the mineral ore such as coal, gold or copper, which is converted to the products (Equation (1)) by either chemical or microbial reactions. The other sources of AMD include the sand and slime dumps resulting from tailings. These dumps have been subjected to oxygenated rainwater, resulting in the oxidation of the residual sulphide containing minerals.

doi: 10.2166/wst.2016.259

A further oxidation occurs on the Fe^{2+} (Equation (1)) to form stable Fe^{3+} ions, which in turn, oxidize the FeS_2 (Equation (1)), as stated by Baker & Banfield (2003), as represented by Equation (2):

$$FeS_2 + 7Fe^{3+} + 13H_2O \rightarrow 8Fe^{2+} + 0.5\ S_4O_6^{2-} + 6H^+ \qquad (2)$$

It is evident from Equations (1) and (2) that a high volume of AMD is generated as oxidation of FeS_2 occurs in two reactions. The research which has been explored has mainly been based on the reduction/removal of the turbid materials (turbidity or total suspended solids (TSS)) and overlooking the chemical reactivity of the reagents (coagulants/flocculants) to induce destabilization, an approach which is invaluable in wastewater treatment. On the other hand, the investigation about the reactivity of the reagents is also vital, which is also determined by their physico-chemical properties. It has to be noted that the effectiveness of the wastewater treatment is governed by the destabilization-hydrolysis reaction, a reaction which is influenced by the chemical reactivity and the adsorption potential of the surfactant/flocs. The type of colloids, i.e. hydrophilicity (water-loving) or hydrophobicity (water-hating), plays a pivotal role during the chemical reactions during treatment (Arabi & Nakhla 2008; Nermen *et al.* 2009). The diversified technological approach employed in AMD treatment includes distillation, reverse osmosis, carbon nanotubes, Fenton's reagent, wet oxidation, advanced oxidation and coagulation–electro-oxidation. These techniques are complex, incur high costs and do not cover a wide range of the wastewater poor quality. Apart from new technologies, lime- and dolomite-neutralization, iron oxidation, gypsum crystallization and activated carbon are common treatment techniques (Geldenhuys *et al.* 2001; Naicker *et al.* 2003; Petrik *et al.* 2003; Semerjian & Ayoub 2003; Chang & Yu 2004; Feng *et al.* 2004; Maree 2004; Watten *et al.* 2005; Akcil & Koldas 2006; Kurniawan *et al.* 2006; Sabah & Erkan 2006; Herrera *et al.* 2007; Arabi & Nakhla 2008; Meghzili 2008; Burgess *et al.* 2009; Sibrell *et al.* 2009). However, the study by Johnson & Hallberg (2005) and Balintova & Petrilakova (2011) revealed that the use of alkaline reagents produces large volumes of hazardous concentrated sludge requiring further treatment and controlled final disposal. In some biological system exploits, the hydrogen sulphide is produced by sulphate-reducing bacteria in order to precipitate metals as sulphides at the various values of AMD pH (Macongova & Luptakova 2012). There are more complicated technologies, such as co-treatment of AMD solution with municipality wastewater using activated sludge (Bratby 2006; Santos *et al.* 2011). Sewage effluent with relatively high concentrations of suspended solids may enhance iron oxyhydroxide precipitation by encouraging iron, which is often present in high concentrations in AMD, to form flocs (Johnson *et al.* 2006; Neto *et al.* 2010; Winfrey *et al.* 2010). Phosphate, which is present in high concentrations in sewage effluent, can be sorbed onto the iron oxyhydroxide precipitates (Sibrell *et al.* 2009; Wei *et al.* 2009, 2010), or react with aluminium to form hydroxyl-phosphates (Johnson *et al.* 2006). Some other researchers, such as Metcalf & Eddy (2003), Bolto & Gregory (2007), Molony (2005), Amuda *et al.* (2006) and Ghaly *et al.* (2006), employed their technologies in wastewater clean-up, an approach which is also applicable to AMD. In conventional AMD treatment, a variety of commercial coagulants, coagulant-aids, flocculants and polyelectrolytes/polymers were employed, some of which are expensive to process as they are prepared in special reactors using special additives (Jiang & Graham 1997). In the present study, the reagents which are used (clay, $FeCl_3$ and $Mg(OH)_2$) are of natural origin, affordable and easy to prepare. The study conducted by Ntwampe *et al.* (2015a) on the AMD sample with $FeCl_3$-$Mg(OH)_2$ polymer dosage using both rapid mixing and shaking respectively, without clay, showed that the turbidity removal efficiency of the polymer was in a range of 91.6–93.7% (rapid mixing) and 90.3–96.9% (shaking). Unlike in this study, clay has always been used as a reagent on its own in the previous studies (Rauf *et al.* 2003; Naseem & Tahir 2004; Gitari *et al.* 2006; Tahir & Naseem 2007; Gitari *et al.* 2011); hence, it is a novel idea to pursue an investigation in which it is used in the form of a polymer. The advantage of adding clay in the polymer is its feldspar component, which is a fluxing agent. The feldspar content was initially altered by hydrolysis during weathering of the rocks to form clay mineral phases such as kaolinites and smectites, where the latter is a principal mineral constituent found in bentonite clay. The clay materials are composed of solid, liquid and vapour phases, where the solid phases are of mineral and organic phases that make up the framework of the clay materials. The mineralogy can be subdivided into the clay and non-clay minerals, including poorly crystalline, amorphous inorganic phases. However, most clay materials are composed of heterogeneous mineral mixtures (Bloch & Hutcheon 1992). The smectites include a group of phyllosilicate mineral species, i.e. montmorillonite, beidellite, nontronite, saponite and hectorite. The chemical composition of these species is characterized by the substitutions of Al for Si in tetrahedral cation sites and Al, Fe, Mg and Li in octahedral cation sites. Smectite clays have a variable net negative charge, which is

balanced by Na, Ca, Mg and/or H adsorbed externally on interlamellar surfaces. Smectite clays are divided into three categories: Na smectites, Ca-Mg smectites and Fuller's or acid earths (Odom 1984).

It is noteworthy that clay does not have valence electrons in its primary formation, but the ions it contains are from the dissolved minerals it absorbed. In a polymeric form (exp A and B), these ions interacted with other ions, whereas the Fe^{3+} and Mg^{2+} ions of the $FeCl_3$ and $Mg(OH)_2$, respectively, interacted with the AMD sample. The valence determines the ionic strength of a metal ion (of a salt) used in the destabilization of the colloidal particles: a process which includes double layer compression. This explains the reaction where by the electrostatic forces of repulsion are reduced and the van der Waals forces of attraction are increased, thus inducing the kinetic movement of the ions through the diffuse layer (Figure A1, available with the online version of this paper).

There are various types of polymers which have been introduced in AMD treatment, but their hydrophilic or hydrophobic properties have not been investigated, a subject which is deliberated in this study. This investigation is based on the adsorption efficiency by the cake-like structures of the synthetic acid-free polymers as shown by the scanning electron microscope (SEM) micrographs in the study by Ntwampe *et al.* (2013), stating that the changes in membrane hydrophobicity/hydrophilicity are influenced by modifications of some of the properties, such as pore size and morphology (Pinnau & Freeman 2000).

It is suggested that the destabilization induced by the clay is predominantly by screening, which also includes neutralization due to charge density (ionic pores). The clay is finely pulverized and the minerals are liberated throughout with varying reactivity potential, and it is therefore imperative to determine the effectiveness between the screening and charging effects, the reactions which correspond to the clay and $FeCl_3$/$Mg(OH)_2$, respectively. A distinctive characteristic of the multivalent polyelectrolytes is that the suspensions form aggregates rapidly near the isoelectric point (IEP), whereas the aggregates slow down away from this point (Gilles *et al.* 2007; Schwarz *et al.* 2007; Szilagyl *et al.* 2011; Sadegpour *et al.* 2011). The IEP is the pH at which a molecule carries no net electric charge, causing neutrality on the charge of the materials in the wastewater, depending on the nature of the colloids and the concentration of other materials (Water Specialist Technology 2003). The condition which separates the slowing aggregation regime due to a low concentration of the particles and fast aggregation caused by high concentration of particles is termed critical coagulation concentration, a transition when the interparticle forces are dominated by the van der Waals forces of attraction and electrostatic double-layer repulsion (Ehrl *et al.* 2009; Chen & Elimelech 2009). During these phenomena, the negatively charged particle surface and the positively charged or electrical neutrality of the bulk of the solution create a potential gradient between the particle surface and a point in the bulk of the solution at some distance away (Coulomb's force of attraction). The distance of such a point can be calculated exactly from a derivation of the Boltzman-Poisson equation, expressed as thickness of the double layer (Figure A2, available with the online version of this paper).

$$\Delta\psi = K^2\psi = \frac{\psi}{\delta^2} \tag{3}$$

where $\Delta\psi$ = potential gradient, K = Boltzman constant and δ = thickness of the double layer.

These equations showed that colloidal stabilization depends on physico-chemical parameters.

Apart from the physico-chemical properties of both the wastewater and the coagulant/flocculent, the colloidal transportation and hydrodynamic interactions play a pivotal role in wastewater treatment. In considering particle transport and collision, three mechanisms are significant to the effect of effective dispersion to induce destabilization-hydrolysis, namely perikinetic and orthokinetic collision and differential sedimentation (Elimelech *et al.* 1995). These are the reactions which determine the effectiveness of the turbidity removal efficiency in the wastewater. The effectiveness of mechanisms depends on the intensity of the mechanical agitation employed to disperse the reagents throughout the solution, as shown by the particles' movement in Figure A2.

All the reagents (clay, $FeCl_3$ and $Mg(OH_2)$) in this study have been used in previous research work (Ntwampe *et al.*, 2015b), but in different polymeric formations compared with those in this study. This includes the acid free-polyferric chloride (af-PFCl) of $Mg(OH)_2$ (exp A) and the clay-(af)-PFCl of $Mg(OH)_2$ (exp B). The rationale of this study is to determine the extent to which their physico-chemical properties effect the removal of turbid materials through the destabilization-hydrolysis reaction. The TSS values and the crystal morphology (SEM micrograph) of the supernatant and the sludge of the AMD samples, respectively, will serve as the source of such an investigation. Both polymers were prepared by mixing the reagents in demineralized water without any additives or catalysts, contributing to the novelty of this study. Based on the simplicity of the

Table 1 | Ionic strength of Fe^{3+} and Mg^{2+} in their standard solutions

Species	Ionic strength
Fe^{3+}	0.193
Mg^{2+}	0.086
$Fe^{3+} + Mg^{2+}$	0.323

preparation, an inference is that the destabilization is more likely to involve both physical and chemical phenomena. It is more likely that the presence of Fe^{3+} ions, a metal ion with a high destabilization-hydrolysis potential (Wulfsberg 1987), as shown in Table 1, contributes enormously in the removal of turbid materials.

The main objective in this study is to investigate key parameters which contribute to effective destabilization, hydrolysis, nucleation, aggregation and sedimentation. Another focus in the present study is to investigate the impact of the polymers which contain clay, Fe^{3+} or Al^{3+} and Mg^{2+} on the destabilization-hydrolysis process for the AMD sample.

The novelty in this study is to determine the TSS removal potential of clay when it reacts with the AMD sample alone compared with when it reacts in a polymeric form. The results of the study will confirm the polymeric strength of a synthetic flocculent (clay, $FeCl_3$ and $Mg(OH)_2$) which was prepared without processing (pre-polymerization or co-polymerization), which is costly, as it requires specialized reactors and acid which has to be partially hydrolyzed.

MATERIALS AND METHODS

In this study, coagulation–flocculation treatment has been employed to the AMD sample using 5 g of clay (bentonite) added to 1.2 L of AMD and treated in a jar test at 250 rpm for 2 min and reduced to 100 rpm for 10 min. A 200 mL supernatant was poured into five 500 mL glass beakers and dosed with a polymer of 5 g clay and 0.1 M $FeCl_3$-$Mg(OH)_2$, i.e. 0.1 Fe^{3+} in $FeCl_3$ and 0.1 M Mg^{2+} in $Mg(OH)_2$. The samples were allowed to settle for 1 h, after which the pH, TSS, dissolved oxygen (DO) and oxidation reduction potential (ORP) of the supernatant were measured.

AMD sample

The samples were collected from the Western Decant in Krugersdorp in a 25 L plastic drum. The sample was airtied and stored at room temperature. The pH, conductivity, turbidity, TSS, ORP and DO of untreated AMD sample were 2.08, 4.94 mS/cm, 252 g/L (105 NTU), 252 g/L, 234 mV and 4.5 mg/L, respectively. The major elements in the AMD measured by the inductively coupled plasma (ICP) are as shown in Table 2.

Table 2 | Printout of ICP results of the untreated AMD sample

Element	Conc. (ppm)
Al	1.17129
Ca	182.128
Co	0.13344
Cu	0.14232
Fe	28.3576
K	4.59173
Mg	67.3925
Mn	35.3678
Na	44.5720
Ni	0.44315
Pb	0.60598
Sr	0.27041
Se	0.71129
Zn	0.34889

Clay sample

The type of clay used in the experiments was pulverized bentonite with the properties shown in Table 3.

Coagulants

Inorganic coagulants of 0.10 M of Fe^{3+} and Mg^{2+} ions were dosed for coagulation-flocculation of the AMD, and the concentration was not related to any study conducted before.

The calculation of the mass of metal salt to obtain 0.10 M of M^{n+} ($M^{n+} = Fe\ or\ Mg$) was as follows:

Monoprotic metal salts (MCl_3)

$$0.10\ M \text{ of } M^{3+} \times \text{mass of } M^{*}Cl_3 6H_2O \quad (M^{*} = Fe) \tag{4}$$

$$0.10\ M \text{ of } Mg^{2+} \times \text{mass of } M^{*}(OH)_2 \quad (M = Mg) \tag{5}$$

Table 3 | Properties of the clay and AMD sample

Sample	pH	Cond (mS/cm)	TSS (g/L)	DO (mg/L)	ORP (mV)
Clay	2.15	2.66	13.6	5.8	230
Raw AMD	2.08	4.94	105	4.5	234

Table 4 shows the monoprotic metal salts dosed into the AMD samples.

Procedure in jar tests

The equipment used for the jar tests was a BIBBY Stuart Scientific Flocculator (SW1 model), which has six adjustable paddles with rotating speeds between 0 and 350 rpm. A 200 mL sample of AMD containing 6.3 g of solid particles was poured into each of the five 500 mL glass beakers for the test. Rapid mixing was set at 250 rpm for 2 min, followed by slow mixing at 100 rpm for 10 min, a normal standard recommended in a jar test.

EXPERIMENTS AND EVALUATIONS

The AMD sample with a dosage of clay and af-PFCl polymer of $Mg(OH)_2$

Five grams of clay (bentonite) was added to 1.2 L of AMD and treated in a jar test at 250 rpm for 2 min and reduced to 100 rpm for 10 min (exp A). Then, 200 mL of the supernatant from exp A was poured into five 500 mL glass beakers and treated with 20–60 mL of a polymer of 5 g of clay and 0.1 M of $FeCl_3$-$Mg(OH)_2$ (exp B). The samples were allowed to settle for 1 h, after which the pH, TSS, DO and ORP of the supernatant were measured.

The AMD sample with a dosage of af-PFCl or $AlCl_3$ polymer of $Mg(OH)_2$

A similar set of experiments was conducted on the AMD sample with a polymer of $FeCl_3$-$Mg(OH)_2$ and $AlCl_3$-$Mg(OH)_2$ dosage respectively; similar jar test methodology and measurement were conducted.

Performance evaluation

The pH was used as a determinant to assess the rate of hydrolysis and hydrolytic potential of the coagulants (Fe^{3+} and Mg^{2+} salts) at different mixing duration, whereas the conductivity and turbidity were measured to determine the ionic potential and removal of colloidal particles from the samples.

Table 4 | Metal salts and metal hydroxide dosed into AMD sample

Salt	Mass of salt (g)	Conc (mol/L)	M^{3+}conc (M)
$FeCl_3$	7.0	0.043	0.043
$Mg(OH)_2$	2.49	0.043	0.043

pH measurement

A SensoDirect Multimeter (made in South Africa) pH/ORP/DO/CD/TSS meter with an electrode filled with silver chloride solution and the outer glass casing membrane covering at the tip was used. The equipment was calibrated with standard solutions with pH of 4.0 and 7.0 before use.

Conductivity

The same instrument was used. The CD probe was connected and the measurement was selected using the button, and the CD reading was displayed.

DO

The same instrument was used. The DO probe was connected and the measurement was selected using the button, and the DO reading was displayed.

ORP

The same instrument was used. The ORP probe was connected and the measurement was selected using the button, and the ORP reading was displayed.

Turbidity measurement converted to TSS measurement

A Merck Turbiquant 3000 T Turbidimeter (made in Japan) was used to determine turbidity or the suspended particles in the supernatant, using Nephelometric Turbidity Unit (NTU) as a unit of measure. It was calibrated with 0.10, 10, 100, 1,000 and 10,000 NTU standard solutions. The values obtained were multiplied by 2.4 to convert to TSS (g/L).

Sludge sample characterization

The sludge of the AMD samples was crushed to a fine particle size and the samples were characterized using X-ray diffraction (XRD) and SEM techniques to determine the phases of the elements/metals and the crystal morphology of the samples.

RESULTS

Figure 1 shows the relationship between the concentration of the metal ions (M^{n+}) in the respective salt and the pH, DO and ORP of AMD sample in exp A and B.

Figure 2 shows the relationship between the concentration of the metal ions (M^{n+}) in the respective salt and the pH, ORP, DO and conductivity of the AMD samples in exp A and B.

Figure 3 shows the concentration of the metal ions (M^{n+}) in the respective salt and the pH, ORP, DO and TSS of the AMD samples in exp A and B.

Figure 4 shows the relationship between the TSS removal efficiencies and the pH of AMD samples in exp A.

Figure 5 shows the relationship between the TSS removal efficiencies and the pH of the AMD samples in exp B.

Figure 6 shows the SEM micrograph of the sludge of the AMD sample in exp A.

Figure 7 shows the SEM micrograph of the sludge of the AMD sample in exp B.

Figure 8 shows the SEM micrograph of the bentonite clay.

Figure 9 shows the SEM micrographs of bentonite clay of 220 and 180 μm particle size.

Figure 10 shows the particle size distribution of the AMD sample.

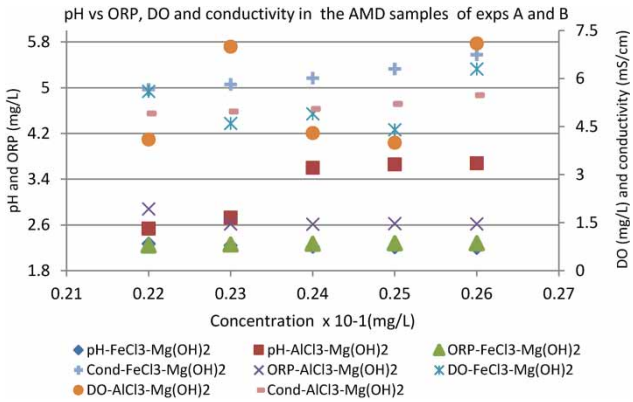

Figure 2 | The concentration of the metal ions in the polymers vs pH, ORP, DO and conductivity.

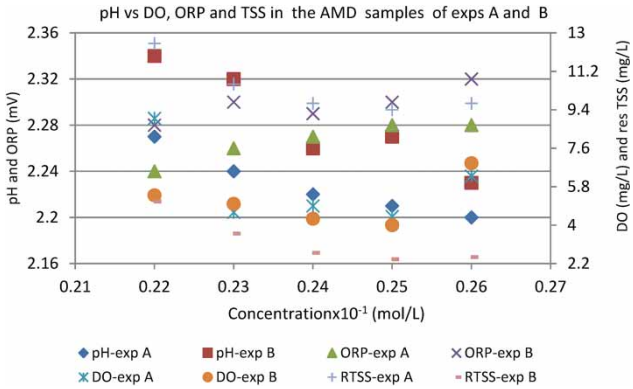

Figure 3 | The concentration of the metal ions in the polymers vs pH, ORP, DO and residual TSS, where RTSS = residual TSS.

DISCUSSION

The experimental results (Figure 3) show that the shear forces, which induce collision of the colloidal particles resulting in rupture, were not severe in both sets of experiments. The results also indicate that the diffusion which occurred during the chemical reactions obeyed Fick's law

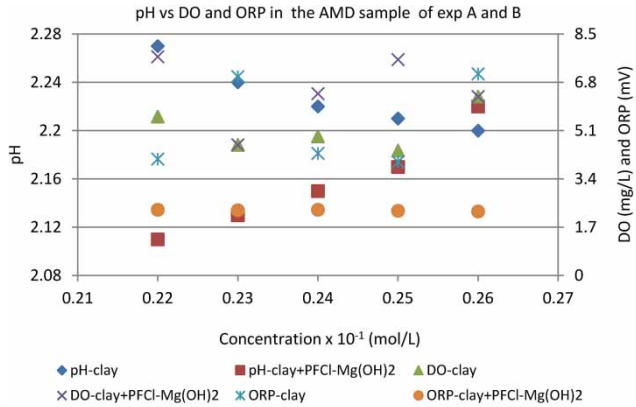

Figure 1 | The concentration of the metal ions vs the pH, DO and ORP in AMD sample in exp A and B.

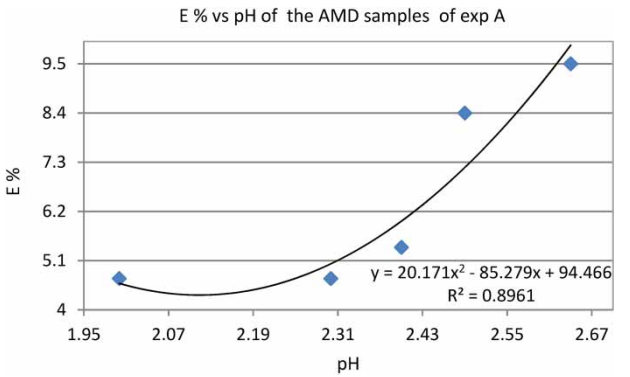

Figure 4 | The E % of TSS vs the pH of AMD samples in exp A.

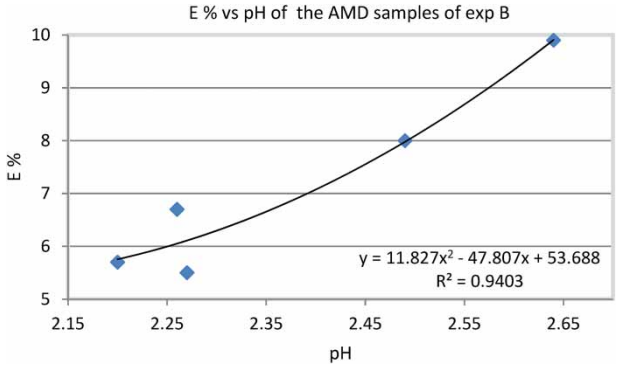

Figure 5 | The E % of TSS vs the pH of AMD samples in exp B.

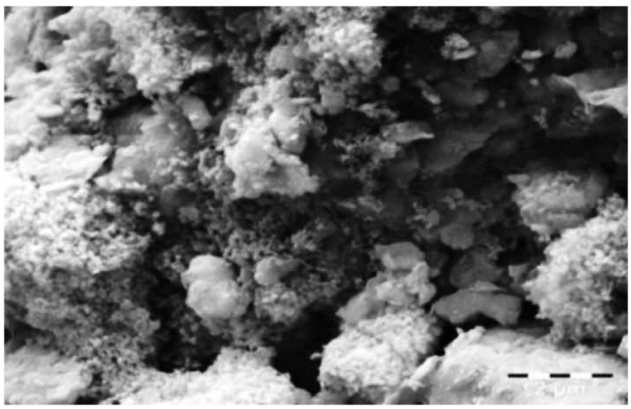

Figure 6 | The SEM micrograph of the sludge of the AMD sample in exp A.

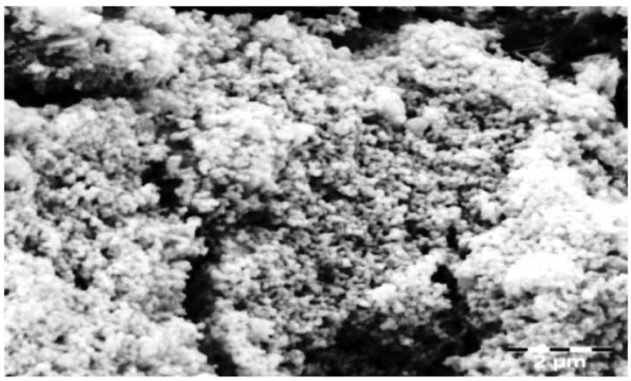

Figure 7 | The SEM micrograph of the sludge of the AMD sample in exp B.

(Equation (6)), showing that the dispersion of the flocculent is uniform and evenly distributed throughout the AMD samples.

Fick's law of the number of particles, *J'*, going through a unit area to a reference particle per unit time was applied,

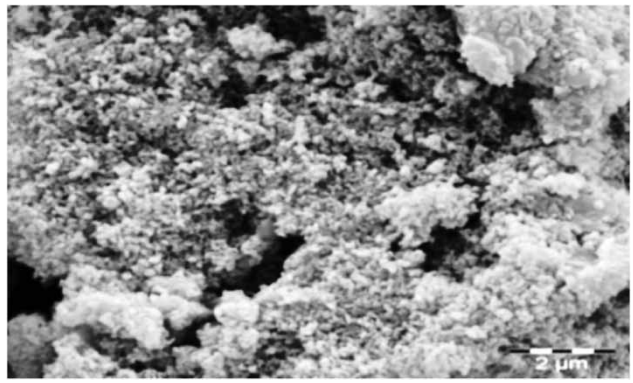

Figure 8 | The SEM micrograph of the clay.

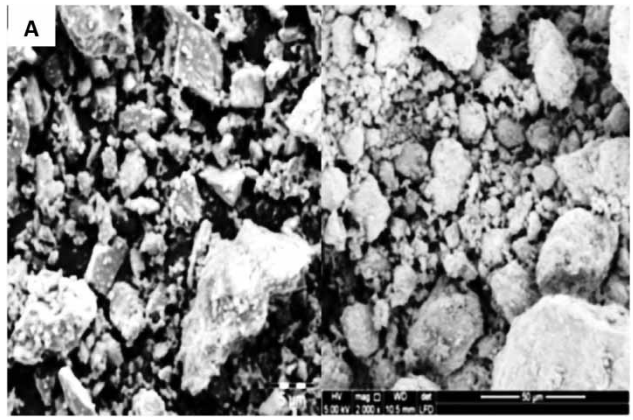

Figure 9 | SEM micrographs of bentonite clay of 220 and 180 µm particle size.

Equation (6).

$$J' = -D\frac{dN}{dr} = -D\frac{dC}{dr} \tag{6}$$

where D = diffusion coefficient (area/time), N = number of concentration and r = radial distance from the centre of the reference particle. It has to be noted that Fick's law applies in a beaker (jar test) when the metal ions diffuse into the system (AMD) and the resultant flocs settle, causing a high concentration at the bottom due to differential velocity. This is shown by the TSS removal efficiency (Figure 3), confirming that there was uniform distribution of diffusion flux (Agarwal 2002).

Effective collision occurs when there are minimal shear forces within the system, and results in the formation of larger particles (Figure 2). It is suggested that the Stern layer (Figure A1) prevents the ions situated in the centre of the aqua-particle from reacting with thions of the neighbouring aqua-particles, which also inhibits the interaction

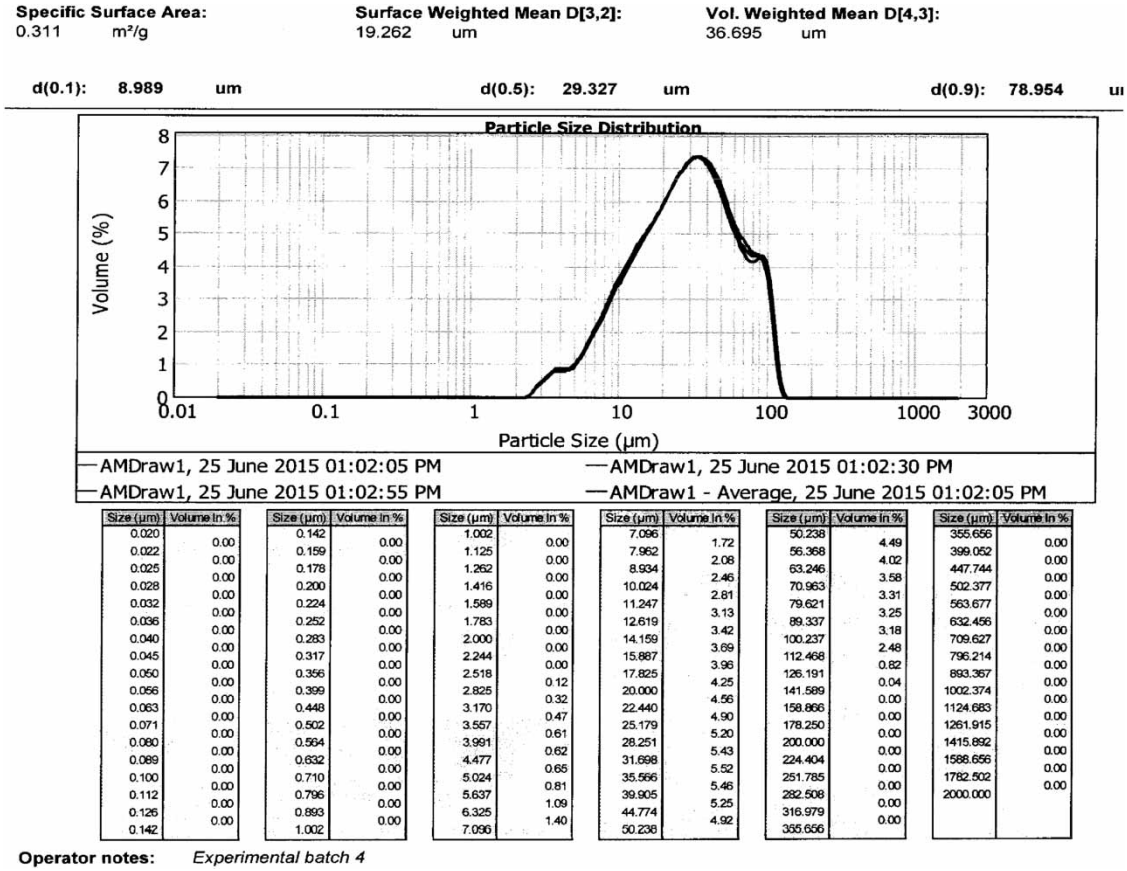

Figure 10 | Particle size distribution of the AMD sample.

with the metal ions (M^{n+}) of the salt. However, the effect of the bipolarity of the water molecules beyond the shear plane together with the ionic strength of the flocculent activate particle-particle interactions (aqua-particle and metal ions) plays a major role as it carries an electrostatic potential, and the electrostatic potential of the shear plane is expressed by Equation (7).

$$Z_n = \frac{4\pi qd}{D} \tag{7}$$

where q = charge of the particle, d = thickness of the layer surrounding the shear plane and D = dielectric constant of the liquid.

Equation (7) indicates the significance of the particle collision due to electrostatic potential to effect destabilization (Figure 3) in the destabilization-hydrolysis reaction. The latter plays a pivotal role in the destabilization-hydrolysis because of the stoichiometric effect (colloids-metal ions) (Steven 1988).

The pH in exp A increased in a decreasing trend from 2.08 (untreated AMD) to a range of 2.27–2.20 with increasing dosage (20–60 mL). It clearly shows that the rate of hydrolysis is determined by the rate and the degree of the destabilization, whereas the pH changing trend determines the hydrolysis reaction, which is a process which includes deprotonation of the solvated metal ions to form metal hydroxide species in a solution. Since there is 0.1 M of Fe^{3+} and Mg^{2+} in their salts, the pH values are ideally representative of an effective destabilization-hydrolysis. Despite the fact that both metal ions share the molar concentration (0.1 M), it is expected that the metal ion with higher valence and that is more acidic dominates the hydrolysis reaction, as shown by decreasing pH values with dosage (Ives 1978); see Equations (8)–(10). However, Fe^{3+} ions undergo hydrolysis to produce species in Equation (8), precursors to the species in Equation (9), due to more acidic property (Wulfsberg 1987):

$$Fe^{3+} + H_2O \rightarrow Fe(OH)^{2+} + H^+_{(aq)} \tag{8}$$

$$Fe^{3+} + 2H_2O \rightarrow Fe(OH)^+_2 + 2H^+_{(aq)} \tag{9}$$

$$Fe^{3+} + 3H_2O \rightarrow Fe(OH)_{3(s)} + 3\ H^{+}_{(aq)} \quad (10)$$

$$Mg(OH)_2 \rightarrow Mg^{2+}_{(aq)} + 2OH^{-}_{(aq)} \quad (11)$$

A higher hydrolysing potential of the Fe^{3+} yielded a higher rate of protonation compared with the rate of OH^- release from the $Mg(OH)_2$ to the system; hence, a slight increase in the pH values is observed (Figure 1).

On the contrary, the pH values in exp B showed an increasing trend with increasing dosages, in a range of 2.11–2.23. The values obtained in exp B are slightly lower compared with those of exp A. It has been mentioned that the clay has ionic pores due to the mineral content adsorbed during the transportation process. The OH^- suppression from increasing the pH in (B) indicates that there is a deficiency of the OH^- ions, and hence pH decreased. It is suggested that some of the OH^- ions from the $Mg(OH)_2$ were adsorbed onto the pores of the clay during polymerization, resulting in a low concentration of the OH^- ions in the system.

The ORP values, the rate at which redox reaction occurs, showed that oxidation took place from 238 mV (untreated AMD) to an increasing trend in exp A in a range of 224–228 mV, whereas the values in (B) showed a decreasing trend in a range of 232–226 mV. According to Equations (1) and (2) (state of AMD sample prior to dosing), it is evident that the oxidation of the Fe^{2+} ions in both reactions was completed and any apparent oxidation may be on the metals in the AMD samples (Table 2) to form precipitates. Another source of oxidation is more likely to be the iron hydrolysis species manifested during speciation ($Fe(OH)^{2+}$ and $Fe(OH)^{+}_{2}$). The high rate of oxidation represented by the values in exp A indicates that the reducing potential of the metals in the AMD samples after the treatment in exp A is lower than the oxidizing potential of exp B. On the contrary, the ORP in the AMD samples in exp B is slightly higher compared with the ORP in the AMD supernatant in (A).

It can be suggested that the morphological structure of the polymer of exp B causes partial hydrolysis of Fe^{3+}, thus reducing the concentration of hydrolysis species which are subjected to oxidation as in (A).

The DO values in the AMD supernatant in (A) are equal to and above 4.5 mg/L (untreated AMD) to a range of 4.5–6.3 mg/L (Figure 1), where only the sample with 50 mL dosage yielded 4.5 mg/L. On the other hand, the DO values in the AMD supernatant in exp B showed a decreasing trend in a range of 7.7–6.3 mg/L. This indicates that the rate at which oxygen reacted in the system (oxidation) in exp A is higher compared with that in exp B. This correlates to the comparison in the ORP values between exp A and B, when it was explained that the rate of oxidation in the former (lower values) is faster compared with the latter (higher values).

The conductivity of the AMD supernatant is more likely to be contributed by the conjugate bases of the metal salts ($FeCl_3$ and $Mg(OH)_2$), because these are the only metal salts which dissolved in the solution. However, only Cl^- ions add to conductivity when the OH^- ions increase the pH of the solution. The conductivity values in (A) exhibited similarly identical values compared with those in (B). This indicates that the addition of the clay to the AMD sample either as a reagent (A) or in a polymeric form (B) (clay-PFCl-$Mg(OH)_2$), did not have any influence on the conductivity during the treatment.

Effective collision (low shear forces) and destabilization are the key factors which determine optimal removal of the turbid materials. The reagent(s) added to the colloidal suspension must have a strong destabilization potential which is able to compress the double layer (Stern and diffuse) (Figure 1) in order to achieve optimal turbidity/TSS removal. Fick's law (Equation (6)) states that the particles with their centres inside the boundary of the reference particle (Figure 2) collide to form aggregates (Agarwal 2002). The collision frequencies are induced by the strength of the reagents by weakening the repulsive forces and reduce the distances between neighbouring aqua-colloids (Equation (6)), with subsequent formation of larger aggregates (settleable). These aggregates either settle or are adsorbed by the substrates (turbidity/TSS removal), as represented in Figure 3. Physico-chemical properties of the reagent(s) and the thickness as well as ionic strength of a colloidal suspension are attributes to optimal turbidity removal, which are expressed by Equation (3). The physico-chemical parameters and the potential gradient induced by the negatively charged particle surface and the positively charged or electrical neutrality of the bulk solution (Equation (3)) influence the double layer compression, thus enhancing the rate of the destabilization, which results in optimal TSS removal.

Since the thickness of the double layer affects the destabilization potential of reagent(s), Equation (3) reveals a correlation between the destabilization potential (reagent) and the potential gradient, i.e. their direct proportionality. The residual TSS values in the AMD supernatant in exp A and B are relatively low, below 12 g/L, and elucidation of the deviation can be explained by comparing the chemical

reactivity of the clay when added as a reagent (exp A) with its reactivity in a polymeric form (exp B). The results in this present study, where the AMD samples are dosed with a polymer in exp A, showed the TSS removal efficiencies in the range of 87.5–90.3%, whereas the TSS removal efficiencies in exp B are in a range of 94.9–97.3%. The improved TSS removal in the latter is contributed by the presence of the clay in the polymer. The inference about the reactivity of the clay is explained in the following. In exp A, the clay was dosed in the AMD sample (1.2 L) prior to af-PFCl-$Mg(OH)_2$ polymer dosage, and reacted in two ways: (a) it formed passivation around the colloidal particles (AMD), resulting in the reduction of the electrostatic forces of repulsion and increasing the van der Waals forces of attraction (Equation (3)); and (b) the ions of the clay minerals attracted their respective oppositely charged ions to cause destabilization on the equilibrium between van der Waals attractive forces and electrostatic repulsive forces. As the destabilization in both processes (a) and (b) occurred during mechanical agitation, the collision between the charged neighbouring particles resulted in the formation of smaller flocs. The smaller flocs were adsorbed onto the pores of the clay, and some of the smaller flocs which are subjected to velocity gradient and differential velocity during slow mixing (flocculation) formed larger flocs which were trapped in the voids of the clay. When the 200 mL of the AMD samples treated with clay only were treated with af-PFCl-$Mg(OH)_2$ polymer, the colloidal particles inside the voids were re-introduced into the system and reacted with the polymer (destabilization-hydrolysis-adsorption), through particle bridging and entrapment in a precipitate (Sincero & Sincero 2003). This suggests that the physico-chemical characteristics of the clay are the main contributory factors to the improved TSS removal, an observation which is in agreement with the study conducted on the AMD by Ntwampe *et al.* (2015b). The elucidation of the reaction of the clay in a broader spectrum involves its principal component, namely smectite. It is suggested that its characteristics, which include gelatinous texture, complex chemical composition, a large chemically active surface area and a high cation exchange capacity (Odom 1984), play a pivotal role in the removal of the turbid materials. Since the preparation of the polymers (exps A and B) did not include a sophisticated process or thermochemical conversion, the metal ions of the polymer react independently in their original ionic form (valence), i.e. highly electronegative (Wulfsberg 1987). The experimental results confirm that physico-chemical properties of the clay and the Fe^{3+} and Mg^{2+} (valence, ionic radii and electronegativity) played a pivotal role in the TSS removal potential (Figure 3). The overall reaction of the polymers can be explained as a combination of a chemical (destabilization-hydrolysis) and physical (adsorption) phenomena. The turbid materials in the AMD also included minerals; Table 5 shows the residual mineral content after treatment.

Apart from the physico-chemical reaction, which includes destabilization-hydrolysis-adsorption chain reaction, the performance of a polymer plays a pivotal role in wastewater treatment processes. The advantage with unprocessed polymers (such as those used in this study) is their unselective property of particle size, as shown in Figure 10.

According to collision mechanisms, the particle sizes which are actively involved during the chemical reactions (collision-aggregation) are less than 100 μm, as classified according to the three reaction stages, i.e. perikinetic, orthokinetic and differential sedimentation. The mechanical stirring induces collision between the colloidal particles and reagent, whereby the physico-chemical properties of the reactants account for the reaction rate contributed by activated energy (E_a). It is therefore postulated that the rate of reaction depends on both the E_a and physico-chemical properties of the particle-reagent. In a collision mechanism, the reactive molecular collisions are the building blocks of the mechanisms of chemical reactions, where the particle sizes play a major role (Herráez-Aguilar *et al.* 2013). The particle size distribution curve (Figure 10) revealed that only 0.86% had particle sizes greater than 100 μm, and the rest (99.14%) were subjected to collision to form flocs, the adsorption substrates. However, the TSS removal values (Figure 10), which are the determinant of

Table 5 | Selected ICP results of metals in treated AMD sample in exp B

Element	Conc (ppm)
Al	2.18484
Ca	187.990
Co	0.13868
Cu	0.05901
Fe	23.6885
K	5.209.8
Mg	68.3926
Mn	34.4218
Na	46.4412
Ni	0.37524
Pb	0.18922
Sr	0.27041
Se	0.79547
Zn	0.31511

the efficiency of the polymer, indicate that the performance of the polymer is characterized by adsorption and not only collision-aggregation. This corroborates the inference that the physico-chemical properties of the clay minerals play a pivotal role in the removal of turbid material.

It has to be noted that the increase in adsorption of the TSS is due to the surface charge of the adsorbent. It is suggested that the surface of the adsorbent is primarily surrounded with hydronium ions at low pH values, which causes a decrease in the interaction between the metal ions, i.e. Fe^{3+} and Mg^{2+}, and the binding sites, which is contributed by greater attractive forces and therefore higher adsorption (Shivani *et al.* 2011). The increase in adsorption is due to the fact that there are more adsorption sites available due to increased surface area when the dosage is increased (Pandey *et al.* 2012), a condition contributed by clay (Figure 3). The elucidation on adsorption dynamics is implicit if not related to the ionic strength (positive or negative ions). According to (Schäfer *et al.* 2011), the positive ions in aqueous systems are solvated to a higher degree than negative ions; and the negative ions predominate at the interface, either by being excluded from the bulk of the solution, or by increased compaction by adsorption on the particle surface. This was corroborated by the statement that the colloids are negatively charged in their original state.

In Figure 4, the residual E% vs the pH of the AMD samples with $FeCl_3$ and $Mg(OH)_2$ polymer dosage, the correlation coefficient of the two parameters is 89.6%.

In Figure 5, the E% vs the pH of the AMD samples with clay, $FeCl_3$ and $Mg(OH)_2$ polymer dosage, the correlation coefficient of the two parameters is 90.4%.

The SEM micrograph of the polymer of $FeCl_3$ and $Mg(OH)_3$ (Figure 8) showed larger dense flocs with smaller flocs joined by sponge-like structures, whereas the SEM micrograph of the combination of clay, $FeCl_3$ and $Mg(OH)_2$ (Figure 7) showed a uniform sponge-like structure showing some small round structures. The SEM micrograph in Figure 6 exhibits the dense and small flocs separated by some distances from one another, compared with the micrograph in Figure 7, which exhibits a uniformly joint cake-like structure. The structure of the latter shows that there is fine gelatinous matter (smectite) which joined the smaller flocs together. It is suggested that the clay minerals interacted chemically with the metal ions (Fe^{3+} and Mg^{2+}) of the polymer during rapid mixing to form a structure with small flocs joined to form a cake-like image (Figure 7). It is notable that the high TSS removal in the AMD samples with a polymer of exp B is contributed by the matrix of the morphological structure shown by such a SEM image (Figure 7). The SEM micrograph of the clay (Figure 8) showed a slightly similar crystal morphology as in Figure 7 (clay and $FeCl_3$-$Mg(OH)_2$), which indicates that the Fe^{3+}, Mg^{2+} and Cl^- ions are absorbed onto the clay. A slight deviation of the TSS values between exp A and B correlates with a slight variation of the SEM micrographs between exp A and B.

The SEM photomicrographs (Figure 9) illustrate bentonite clay with 180 and 220 μm particle sizes (Table 6) respectively (Figure 9(a) and 9(b)). The mineral content and the weight % in these micrographs are shown in Tables 6 and 7, where CO_2 and FeO, which represent siderite ($FeCO_3$), form a larger wt % (33.2 and 45.3 wt %) of the total complex compounds contained in both coal/gold mineral composition, and the rest are trace elemental compounds. The latter (clay with a particle size of 220 μm) exhibits a dense spherical unreactive structure which can be associated with SiO_2 beneath the uniformly joined small and large structures. Another distinction between the two photomicrographs is that less area is covered by unreactive SiO_2 (Figure 9(a)) compared with Figure 9(a). According to these photomicrographs (9(a) and 9(b)), it can be concluded that the bentonite clay particle size plays a pivotal role in the sorption capacity of the turbid material. The particle size of the sample employed in this study is 220 μm (Figure 9(b)), exhibiting a smaller surface area showing that a smaller quantity of bentonite clay can yield identical turbidity removal efficiencies compared with the performance exhibited by 5 g bentonite clay dosed in the present study (<97.3%). It has to be noted that the AMD contains a low heavy mineral content; the treatment in this is therefore to remove organic and non-organic material (silicates, quartz,

Table 6 | Mineral weight % in bentonite clay of different sizes

Spectrum	C	Na	Mg	Al	Si	K	Ca	Ti	Fe	O
Bent. 220 μm	19.56	0.01	5	0.13	2.37	0.09	10.13	0.02	0.3	62.39
Bent. 60 μm	5.7	0.54	0.93	7.44	23.65	1.46	0.84	0.49	6.55	52.39
Bent. 180 μm	6.28	0.51	0.9	7.12	22.26	1.39	0.77	0.52	7.85	52.4

Bent. = bentonite clay.

Table 7 | Weight and atomic % of the bentonite clay

Element	Weight %	Weight %	Atomic %	Compd %	Formula	No. of ions
C K	9.07	0.46	16.55	33.22	CO_2	2.15
Mg K	0.91	0.08	0.82	1.50	MgO	0.11
Al K	1.56	0.08	1.26	2.94	Al_2O_3	0.16
Si K	5.06	0.13	3.95	10.82	SiO_2	0.51
S K	1.48	0.10	1.01	3.69	SO_3	0.13
Ca K	1.14	0.08	0.62	1.60	CaO	0.08
Ti K	0.53	0.09	0.24	0.89	TiO_2	0.03
Fe K	35.25	0.49	13.84	45.34	FeO	1.79
O	45.02	0.58	61.70			8.00
Total	**100.00**					

soil, etc.). The effluent can be used to extract salts/minerals of higher concentration, i.e. Ca, Mg, Mn, Na, K, Fe and Al (Table 6), after which it can be utilized as neutralizing effluent in alkaline treatment processes. The observations obtained in Figure 9 and Table 6 indicate that bentonite clay of the smaller particle size (180 μm) and smaller quantity (<5 g) can yield a similar TSS removal efficiency compared with those of the bentonite clay employed in this study.

Table 7 shows weight and atomic % of the bentonite clay, showing the mineral compounds contained in bentonite clay.

The Pearson correlation coefficient (r) to calculate the relation between pH and residual turbidity is given in Equation (12).

$$r = \frac{n(\Sigma xy) - (\Sigma x)(\Sigma y)}{\sqrt{[n\Sigma x^2 - (\Sigma x)^2][n\Sigma y^2 - (\Sigma y^2)]}} \quad (12)$$

According to the correlation coefficient, 0.70 or higher is a very strong relationship, 0.40–0.69 is a strong relationship, and 0.30–0.39 is a moderate relationship. The parameters obtained for the E % and pH of the AMD sample with the combination of $FeCl_3$ and $Mg(OH)_2$ (A) compared with the combination of clay, $FeCl_3$ and $Mg(OH)_2$ (B) (Figure 3) are:

$$\Sigma x_{\exp(A)} = 35.8,\ \Sigma x^2_{\exp(A)} = 269.6,\ \Sigma y_{\exp(A)} = 11.9,\ \Sigma y^2_{\exp(A)} = 28.3 \text{ and } \Sigma xy_{\exp(A)} = 86.2$$

$$\Sigma x_{\exp(B)} = 32.7,\ \Sigma x^2_{\exp(B)} = 234.2,\ \Sigma y_{\exp(B)} = 11.8,\ \Sigma y^2_{\exp(B)} = 28.2 \text{ and } \Sigma xy_{\exp(B)} = 79.2$$

The r-value obtained for the AMD samples (Figure 3) in exp A is 0.805 (80.5%) with the range of the correlation coefficient from −1 to 1. The correlation coefficient for the samples thus falls within a range of strong relationship. This is validated by the R^2 of E% vs pH of 0.896 (89.6%), as shown in Figure 3. The r-value obtained for the AMD sample (Figure 3) in exp B is 0.898 (89.8%) and thus also has a strong relationship. This is validated by the R^2 of ORP vs pH of 0.940 (94.0%), as shown in Figure 3.

CONCLUSION

The pH of the sample with clay treatment decreases with increasing mass concentration of the particles in a solution (exp A), whereas the pH of the polymer (clay and $FeCl_3$-$Mg(OH)_2$) increases with increasing mass concentration of the particles in a solution (exp B). The conductivity of the samples with a polymer of $FeCl_3$-$Mg(OH)_2$ exhibits a higher increasing trend with increasing concentration of the particles in a solution compared with the conductivity of the samples with a polymer of $AlCl_3$-$Mg(OH)_2$. The polymers used in exp A exhibited TSS removal efficiency which is slightly lower compared with the polymer used in exp B, above 90%. A larger amount of turbid materials has been adsorbed onto the active sites of the clay, showing that clay has a high TSS removal efficiency. The SEM micrograph of the AMD sludge with the same polymer dosage exhibited a very rigid and compacted structure consisting of smaller flocs bound together. On the contrary, the SEM micrograph of the AMD sludge with a polymer of exp A exhibited dense and smaller flocs joined together by sponge-like structures; the micrograph showed some spaces in between the dense flocs. The high rate of oxidation represented by the values in exp A indicates that the reducing potential of the metals in the AMD samples of exp A is lower than the oxidizing potential of exp B. On the contrary, it is noted that the ORP in the AMD samples in exp B is slightly higher compared with the ORP in the AMD supernatant in exp A.

ACKNOWLEDGEMENTS

This work is based on the research financially supported by the South African Research Chairs Initiative (SARChI) of the Department of Science and Technology and National Research Foundation of South Africa (Coal Research Chair

Grant No. 86880, UID85643, Grant No. TP1208137225). Any opinion, finding, or conclusion or recommendation expressed in this material is that of the authors and the NRF does not accept any liability in this regard.

REFERENCES

Agarwal, S. 2002 *Efficiency of Shear-Induced Aggregates of Particles Suspension to Bridging Flocculation*. PhD Dissertation, West Virginia University, Morgantown. http:/etd/EDTS/E23/Agarwal_Sushant_dissertation.pdf.

Akcil, A. & Koldas, S. 2006 Acid Mine Drainage (AMD): causes, treatment and case studies. *Journal of Cleaning Products* **14**, 1139–1145.

Amuda, O. S., Amoo, A. & Ajayi, O. O. 2006 Performance optimization of coagulant/flocculant in the treatment of wastewater from a beverage industry. *Journal of Hazardous Materials* **129**, 69–72.

Arabi, S. & Nakhla, G. 2008 Impact of calcium on the membrane fouling in membrane bioreactors. *Journal of Membrane Science* **314**, 134.

Baker, B. J. & Banfield, J. F. 2003 Microbial communities in acid mine drainage. *FEMS Microbiology Ecology* **44**, 139–152.

Balintova, M. & Petrilakova, A. 2011 Study of pH influence of selective precipitation of heavy metals from acid mine drainage. *Chemical Engineering Transaction* **25**, 1–6.

Bloch, J. & Hutcheon, I. E. 1992 Shale diagenesis: a case study from the Albanian Harmon member (Peace River formation). *Western Canada, Clays and Clay Mineral* **40** (6), 682–699.

Bolto, B. & Gregory, J. 2007 Organic polyelectrolytes in water treatment. *Water Research* **41**, 2301–2324.

Bratby, J., 2006 *Coagulation and Flocculation in Water and Wastewater Treatment*. 2nd edn. IWA Publishing, UK.

Burgess, J., De Jong, H. C. & Aguitar, Z. P. 2009 *Biological Nanostructures, Materials, and Applications*. ECS Transaction, New Jersey.

Chang, Q. & Yu, M. 2004 An application of macromolecular heavy metal flocculant in wastewater treatment. *Chemosphere* **6**, 42–47.

Chen, K. L. & Elimelech, M. 2009 Relating colloidal stability of fullerene (C-60) nanoparticles to nanoparticle charge and electro-kinetic properties. *Environmental Science and Technology* **43**, 7270–7276.

Cravotta, C. A. 2008 Dissolved metals and associated constituents in abandoned coal-mine discharges, Pennsylvania, USA: 1. Constituent concentrations and correlations. *Applied Geochemistry* **23**, 166–202.

Edwards, A. C. & Withers, P. J. A. 2007 Linking phosphorus sources to impacts in different types of water body. *Soil Use Manage* **23**, 133–143.

Ehrl, L., Jia, Z., Wu, H., Lattuada, M., Soos, M. & Morbidelli, M. 2009 Role of counterion association in colloidal stability. *Langmuir* **25**, 2696–2702.

Elimelech, M., Gregory, J. & Williams, R. A. 1995 *Particle Deposition and Aggregation: Measurement, Modeling and Simulation.* Butterworth-Heinemann, Elsevier, Oxford.

Feng, D., van Deventer, J. S. J. & Aldrich, C. 2004 Removal of pollutants from acid mine wastewater using metallurgical by-product slags. *Separation and Purification Technology* **40**, 61–67.

Firer, D., Friedler, E. & Lahav, O. 2008 Control of sulfide in sewer systems by dosage of iron salts: comparison between theoretical and experimental results, and practical implications. *Science of the Total Environment* **392**, 145–156.

Gallato, S. L., Peterson, M., Alexandre, N. Z., da Costa, J. A. D., Izidoro, G., Sorato, L. & Levati, M. 2009 Incorporacao de residuo do tratamento de drenagem acida em massa de ceramic a vermelha. *Ceramica* **55**, 53–60.

Geldenhuys, A. J., Maree, J. P., Fourie, W. J., Smit, J. J., Bladergroen, B. J. & Tjati, M. 2001 Acid mine drainage treated electrolytically for recovery of hydrogen, iron(II) oxidation and sulphur production. Submission at the 8th International Congress on Mine Water & Environment in Johannesburg, South Africa.

Ghaly, A. E., Snow, A. & Faber, B. E. 2006 Treatment of grease filter washwater by chemical coagulation. *Canadian Biosystem Engineering* **48**, 6.13–6.22.

Gilles, G., Kin, W. & Borkovec, M. 2007 Charging aggregation of negatively charged latex particles on the presence of anionic polyelectrolytes. *Journal of Physical Chemistry* **111**, 8626–8633.

Gitari, M. W., Petrik, L. F., Etchebers, O., Key, D. L., Iwuoha, E. & Okujeni, C. 2006 Treatment of acid mine drainage with Fly ash: removal of major contaminants and trace elements. *Journal Environmental Science Health-Part A* **41** (8), 1729–1747.

Gitari, W. M., Kaseke, C. & Nkuzani, B. B. 2011 Passive remediation of acid mine drainage using bentonite clay: a laboratory batch experimental study. *International Mine Water Association*, 325–330.

Gupta, R. 2007 Advanced coal characterization: a review. *Energy & Fuels* **21**, 451–460.

Hallberg, K. B. 2010 New perspectives in acid mine drainage microbiology. *Hydrometallurgy* **104**, 448–453.

Herráez-Aguilar, D., Jambrina, P. G., Aldegunde, J., Sáez-Rábanos, V., de Miranda, M. P. & Aoiz, F. J. 2013 The reactive collision mechanism evinced: stereodynamical control of the elementary Br + H2 → H + HBr reaction. *Phys. Chem. Chem. Phys.* **15** (32), 13513–13522. doi: 10.1039/c3cp51271a.

Herrera, P. S., Uchiyama, H., Igarashi, T., Asakura, K., Ochi, Y., Ishizuka, F. & Kawada, S. 2007 Acid mine drainage treatment through a two-step neutralization ferrite-formation process in northern Japan: physical and chemical characterization of the sludge. *Mineral Engineering* **20**, 1309–1314.

Hower, J., Graham, U. M., Dozier, A., Tseng, M. T. & Khatri, R. A. 2008 Association of the sites of heavy metals with nanoscale carbon in a Kentucky electrostatic precipitator fly ash. *Environmental Science and Technology* **42**, 8371–8477.

Huang, X. & Finkelman, R. B. 2008 Understand the chemical properties of macerals and minerals in coal and its potential application for occupational lung disease prevention. *Journal of Toxicological Environmental Health, Part B* **11**, 45–67.

Ives, K. 1978 *The Scientific Basis of Flocculation.* Sijthoff & Noordhoff, The Netherlands, pp. 81–112.

Jiang, J. Q. & Graham, N. J. D. 1997 *Chemistry & Industry*, Springer-Verlag, Berlin.

Johnson, D. B. & Hallberg, K. B. 2005 Acid mine drainage remediation options: a review. *Science of the Total Environment* **338**, 3–14.

Johnson, Z. I., Zinser, E. R., Coe, A., McNulty, N. P., Woodward, E. M. & Chisholm, S. W. 2006 Niche partitioning among Prochlorococcus ecotypes along ocean-scale environmental gradients. *Science* **311**, 1737–1740.

Kurniawan, T. A., Chan, W. S., Lo, W.-S. & Babel, S. 2006 Physico-chemical treatment techniques for wastewater laden with heavy metals. *Chemical Engineering* **118**, 83–87.

Macongova, E. & Luptakova, A., 2012 Recovery of metals from acid mine drainage. *Chemical Engineering Transaction* **28**, 109–114.

Maree, J. P. 2004 Treatment of industrial effluent for neutralization and sulphate removal, A thesis submitted for PhD at the North West University, RSA.

Meghzili, B. 2008 Tests of coagulation–flocculation by aluminum sulphate and polycations Al on raw waters of the station of treatment Skikda (Algeria). *European Journal Scientific Research* **23** (2), 268–277.

Metcalf, W. & Eddy, C. 2003 *Wastewater Engineering*, 4th edn. McGraw-Hill Inc., New York.

Molony, J. 2005 *Colour Coating & Corrosion SA-J. for OCCA SA, SAPMA*. Leaf Media, Natal, SA.

Naicker, K., Cukrowska, E. & McCarthy, T. S. 2003 Acid mine drainage from gold mining activities in Johannesburg, South Africa and environs. *Environmental Pollution* **122**, 29–40.

Naseem, R. & Tahir, S. S. 2004 Removal of Fe(II) from the wastewater of galvanized pipe manufacturing industry by adsorption onto bentonite clay. *Journal of Environmental Management* **73**, 285–292.

Nermen, M., Nakhla, G. & Wan, W. 2009 Comparative assessment of hydrophobic and hydrophilic membrane fouling in wastewater applications. *Journal of Membrane Science* **339** (1), 93–99.

Neto, M. A. S., Villwock, R., Scheer, S., Steiner, M. T. A. & Dyminski, A. S. 2010 Visual data mining techniques applied for the analysis of data collected at Itaipu power plant, Técnicas de Mineração Visual de Dados aplicadas aos dados deinstrument.

Nielsen, A. H., Lens, P., Vollertsen, J. & Hvitved-Jacobsen, T. 2005 Sulfide-iron interactions in domestic wastewater from a gravity sewer. *Water Research* **39**, 2747–2755.

Nielsen, A. H., Vollertsen, J., Jensen, H. S., Wium-Andersen, T. & Hvitved-Jacobsen, T. 2008a Influence of pipe material and surfaces on sulfide related odor and corrosion in sewers. *Water Research* **42**, 4206–4214.

Nielsen, A. H., Hvitved-Jacobsen, T. & Vollertsen, J. 2008b Effects of pH and iron concentrations on sulfide precipitation in wastewater collection systems. *Water Environmental Research* **80**, 380.

Ntwampe, I. O., Jewell, L. L., Hildebrandt, D. & Glasser, D. 2013 The effect of mixing on the treatment of paint wastewater with Fe^{3+} and Al^{3+} salts. *Journal of Environmental Chemistry and Ecotoxicology* **5** (1), 7–16.

Ntwampe, I. O., Waanders, F. B., Bunt, J. R. & Fosso-Kankeu, E. 2015a Reaction dynamics of iron and aluminium salts dosage in AMD using shaking as an alternative technique in the destabilization-hydrolysis process. *International Journal of Science* **4**, 38–55.

Ntwampe, I. O., Waanders, F. B. & Bunt, J. R. 2015b Comparison between mixing and shaking technique during the destabilization-hydrolysis of acid mine drainage (AMD) using $Ca(OH)_2$ and $Mg(OH)_2$. *Journal Chemical Engineering & Material Science* **6** (3), 15–33.

Odom, I. E. 1984 Smectite clay minerals: properties and uses. *Philosophical Transactions of the Royal Society A*, 311 (1517). DOI: 10.1098/rsta.1984.0036.

Pandey, J. K., Kim, H-J., Takegi, H., Lee, C. S. & Ahn, S. H. 2012 Preparation and properties of cellulose-based nano composites of clay and polypropylene. *Journal of Applied Polymer Science* **125** (S1), E651–E660.

Petrik, L. F., White, R. A., Klink, M. J., Somerset, V. S., Burgers, C. L. & Fey, M. V. 2003 Utilization of South African Fly Ash to treat acid coal mine drainage, and production of high quality zeolites from the residual solids. In: *Submission of International Ash Utilization Symposium*, October 20–22, 2003, Lexington, Kentucky, USA.

Pinnau, I. & Freeman, B. D. 2000 *Membrane Formation and Modification*. ACS, Washington, DC.

Rauf, M. A., Iqbal, J., Ikram, M. & Rauf, N. 2003 Adsorption studies of Ni(II) from aqueous solution onto bentonite. *Journal of Trace Microprobe Technology* **21**, 337–342.

Sabah, E. & Erkan, Z. E. 2006 Interaction mechanism of flocculants with coal waste slurry. *Fuel* **85**, 350–359.

Sadegpour, A., Seyrek, E., Szilayi, L., Hierrezuolo, J. & Borkovec, M. 2011 Influence of the ionized charged and molecular mass of weak polyelectrolytes on charging and stabilization behaviour of oppositely charged colloidal particles. *Langmuir* **27**, 9270–9276.

Santos, J. A., Nunes, L. A. P. L., Melo, W. J. & Araujo, A. S. F. 2011 Tannery sludge compost amendment rates on soil microbial biomass of two different soils. *European Journal of Soil Biology* **47**, 146–151.

Schäfer, A. I., Semião, A. & Akanyeti, I. 2011 Micropollutant sorption to membrane polymers, Advances in Colloid and Interface Science. 'Membrane Separation and Colloid Science' invited special issue paper (accepted 09/2010). DOI:10.1016/j.cis.2010.09.0063.

Schwarz, S., Jaeger, W., Paulke, B. R., Bratskaya, N. & Bohrisch, J. 2007 Cationic flocculants carrying hydrophobic functionalities: applications for solid/liquid. *Journal of Physical Chemistry B* **11**, 8649–8654.

Semerjian, L. & Ayoub, G. M. 2003 High-pH-magnesium coagulation-flocculation in wastewater treatment. *Advanced Environmental Research* **7**, 389–403.

Shivani, S., Anukool, S., Negi, M. P. S & Tandon, P. K. 2011 Evaluation of effect of drains on water quality of river Gomti in Lucknow city using multivariate statistical technique. *International Journal of Environmental Science* **2** (2), 1–3.

Sibrell, P. L., Montgomery, G. A., Ritenour, K. L. & Tucker, T. W. 2009 Removal of phosphorus from agricultural wastewaters using adsorption media prepared from acid mine drainage sludge. *Water Research* **43** (8), 2240–2250.

Silva, L. F. O., Monero, T. & Querol, X. 2009 An introductory TEM study of Fe-nanominerals within coal fly ash. *Science of Environment* **407**, 4972–4974.

Silva, L. F. O., Macias, F., Oliviera, M. L. S., Da Boit, K. M. & Waanders, F. 2010 Leaching of potential hazardous elements of coal cleaning rejects. *Environmental Monitoring and Assess*, **172** (1), 367–378. DOI: 10.1007/s10661-010-1340-8.

Sincero, A. P. & Sincero, G. A. 2003 *Physical-Chemical Treatment of Water and Wastewater*. IWA Publishing, London, UK.

Sinha, P., Szilagyi, I., Ruiz-Cabello, F. J. M., Maroni, P. & Borkovec, M. 2013 Attractive forces between charged colloidal particles induced by multivalent ions revealed by confronting aggregation and direct force measurements. *Journal Physical Chemistry* **4** (4), 648–652.

Skalny, J., Marchand, J. & Odler, I. 2001 *Sulfate Attack on Concrete*. E and FN Spon, London, UK.

Steven, K. D. 1988 Application of the precipitation-charge neutralization model of coagulation. *Environmental Science and Technology* **22** (7), 825–832.

Szilagyl, L., Rosicka, D., Hierrezucko, J. & Borkovec, M. 2011 Charging and stabilization of anionic latex particles in the presence of linear poly (ethylene imine). *Journal Colloidal Interface Science* **360**, 580–585.

Tahir, S. S. & Naseem, R. 2007 Removal of Cr^{3+} from tannery waste water by adsorption onto bentonite clay. *Separation and Purification Technology* **53**, 312–321.

Water Specialist Technology 2003 *Jar Test Procedure for Precipitants, Coagulants & Flocculants*. WordPress.Org, Florida, USA.

Watten, B. J., Sibrella, P. L. & Schwartz, M. F. 2005 Acid neutralization within limestone sand reactors receiving coal mine drainage. *Environmental Pollution* **137**, 295–304.

Wei, J., Gao, B., Yue, Q., Wang, Y., Li, W. & Zhu, X. 2009 Comparison of coagulation behaviour and floc structure characteristic of different polyferric-cationic polymer dual-coagulants in humic acid solution. *Water Research* **43**, 724–732.

Wei, J. C., Gao, B. W., Yue, Q. Y. & Wang, Y. 2010 Strength and regrowth properties of polyferric-polymer dual-coagulant flocs in surface water treatment. *Journal of Hazardous Materials* **175**, 949–954.

Winfrey, B. K., Strosnider, W. H., Nairn, R. W. & Strevett, K. A. 2010 Highly effective reduction of faecal indicator bacteria counts in an ecologically-engineered municipal wastewater and acid mine drainage passive co-treatment system. *Ecological Engineering* **36**, 1620–1626.

Wulfsberg, G. 1987 *Principles of Descriptive Inorganic Chemistry*. Brooks/Cole Publishing Company, Mill Valley, CA.

First received 22 March 2016; accepted in revised form 18 May 2016. Available online 6 June 2016